Mean first passage times of higher-dimensional velocity jump processes

Maria R. D'Orsogna*
Department of Mathematics, California State University at Northridge, Los Angeles, CA, 91330, USA and
Department of Computational Medicine, University of California at Los Angeles, Los Angeles, 90095-1766, CA, USA

Alan E. Lindsay
Department of Applied and Computational Mathematics and Statistics,
University of Notre Dame, Notre Dame, IN, 46656, USA

Thomas Hillen
Department of Mathematical and Statistical Sciences,
University of Alberta, Edmonton, T6G 2G1, Canada
(Dated: April 3, 2026)

First passage phenomena arise across physics, biology, and finance when stochastic processes first reach a threshold, triggering downstream events. Examples include the irreversible exit from a domain, a biochemical reaction, a financial selloff. While typical formulations involve diffusive motion, many stochastic processes are better described as velocity jump processes, characterized by persistent motion interrupted by stochastic velocity changes. Despite their ubiquity, first-passage properties of velocity jump processes remain underdeveloped in higher dimensions, especially under directional bias. We present a general framework to estimate the mean first passage time (MFPT) and higher moments of the survival probability for fixed-speed velocity jump processes where possible reorientations range from strong alignment to full angular anisotropy. For low Knudsen numbers, when the mean free path is small compared to the distance to the target, we derive a universal form for the MFPT in which two bias functions encode broad classes of angular distributions, including von Mises–Fisher, wrapped Cauchy, and elliptical families. In the narrow capture limit of a vanishingly small target, directional persistence induces anomalous scaling, including regimes where the MFPT remains finite whereas standard diffusion would predict divergence. Finally, we obtain a Langevin representation that accurately reproduces first-passage statistics. Analytical predictions are confirmed by numerical simulations.

Velocity jump processes capture a wide range of realistic non-diffusive behaviors [1, 2]. Examples include molecular collisions in biochemistry [3], run-and-tumble motion in bacteria [4–8], pricing in quantitative finance [9–11], animal movement [12–15]. In all cases, the items of interest "run" along a given direction for a random time until a new velocity is selected. The resulting dynamics is intermittent directed motion that can significantly differ from standard diffusion due to the inherent persistence. Velocity jumps may arise from internal mechanisms, external perturbations, or in response to sensory cues. The best known representation of this paradigm are the one-dimensional telegrapher equations that are commonly used to study run-and-tumble behaviors [16–19]. Non-equilibrium first-passage properties of jump processes are of great significance and may be even more important than steady-state quantities such as moments of the mean displacement or particle distributions [20]. For example, the mean first passage time (MFPT), defined as the average time to first reach a target [21], informs how long one must wait for downstream, often irreversible, events to be initiated, such as immune responses, biochemical transformations, entry into subcellular compartments [22–24], escape from an enclosed domain [25–27]. The time to reach a threshold is also used as a measure of resilience in ecology [28] or to quantify the onset of mental health disorders [29]. Understanding how persistence and directionality affect first passage phenomena is critical [30–34]; however, the problem is notoriously difficult in higher dimensions because velocities can reorient along a continuum of directions, and not just to the left or right as in $d = 1$ [35–37].

The aim of this Letter is to help fill this gap. We write a general equation for the MFPT $\Theta(\mathbf{x}, \mathbf{v})$ to a given target for a particle starting at position $\mathbf{x}$ with velocity $\mathbf{v}$ under a velocity jump process where jumps occur at rate μ and where $q(\mathbf{x}, \mathbf{v})$ is the memoryless probability density function for a particle at $\mathbf{x}$ to switch to velocity $\mathbf{v}$. In many settings the speed v is fixed, to a physiological value in biology or to the thermal velocity in Brownian motion for example, so that the jump process becomes a series of stochastic reorientations. The turning angle may be completely random, as in run-and-tumble systems, or may bias the motion along a preferred direction, as when there is an underlying network, external field or chemical trail. For fixed speed $v = \sigma$ and small Knudsen number $\varepsilon = \sigma/(\mu L) \ll 1$, where σ/μ is the mean free path and L is a characteristic distance the particle must travel before reaching the target or escaping the domain, we show that $\Theta(\mathbf{x}, \mathbf{v}) \sim T(\mathbf{x}) + \mathcal{O}(\varepsilon)$ and write a self-contained differential equation for $T(\mathbf{x})$ valid in d-dimensional systems. We solve for $T(\mathbf{x})$ under representative turning angle dis-

tributions in simple geometries and compare our results with numerical simulations for $d = 2, 3$.

The probability density $P(\mathbf{x}, \mathbf{v}, t)$ to be at position $\mathbf{x}$ with velocity $\mathbf{v}$ at time t obeys the forward equation

$$\frac{\partial P}{\partial t} + \mathbf{v} \cdot \nabla P = -\mu P + \mu \int q(\mathbf{x}, \mathbf{v}) P(\mathbf{x}, \mathbf{v}', t) d\mathbf{v}' \quad (1)$$

for given initial and boundary conditions. The integral is over the chosen velocity domain of $q(\mathbf{x}, \mathbf{v})$. The survival probability $S(\mathbf{x}, \mathbf{v}, t)$ for a particle initiated at $(\mathbf{x}, \mathbf{v})$ to remain in a spatial domain $\mathcal{D}$ without having reached a specified target at time t follows the backward Kolmogorov equation, given by the adjoint of Eq. 1

$$\frac{\partial S}{\partial t} - \mathbf{v} \cdot \nabla S = -\mu S + \mu \int q(\mathbf{x}, \mathbf{v}') S(\mathbf{x}, \mathbf{v}', t) d\mathbf{v}', \quad (2)$$

where $S(\mathbf{x}, \mathbf{v}, 0) = 1$ for all $\mathbf{x}$ in $\mathcal{D}$ and any $\mathbf{v}$. Eq. 2 is solved with absorbing boundaries at the target and reflecting elsewhere; more details are given in the Supplemental Material (SM). The escape probability $1 - S$ yields the first-passage time probability density $-\partial S/\partial t$. The MFPT $\Theta(\mathbf{x}, \mathbf{v})$ is its first moment

$$\Theta(\mathbf{x}, \mathbf{v}) = -\int_0^\infty t \frac{\partial S}{\partial t} dt = \int_0^\infty S(\mathbf{x}, \mathbf{v}, t) dt. \quad (3)$$

Integrating Eq. 2 over time yields

$$-1 - \mathbf{v} \cdot \nabla \Theta = -\mu \Theta + \mu \int q(\mathbf{x}, \mathbf{v}') \Theta(\mathbf{x}, \mathbf{v}') d\mathbf{v}'. \quad (4)$$

Upon multiplying Eq. 4 by $q(\mathbf{x}, \mathbf{v})$ and by $\mathbf{v}\,\mathbf{q}(\mathbf{x}, \mathbf{v})$, integrating both expressions over velocity space, and merging results one obtains

$$\begin{aligned} -1 \;=\; & \frac{1}{\mu} \int q(\mathbf{x}, \mathbf{v}) (\mathbf{v} \otimes \mathbf{v} : \nabla \otimes \nabla) \Theta(\mathbf{x}, \mathbf{v})\, d\mathbf{v} + \\ & \mathbf{b}(\mathbf{x}) \cdot \nabla \int q(\mathbf{x}, \mathbf{v})\, \Theta(\mathbf{x}, \mathbf{v}) d\mathbf{v}. \end{aligned} \quad (5)$$

Here $\otimes$ represents the tensor product between vectors and the colon their convolution, so that in dimension d

$$\mathbf{v} \otimes \mathbf{v} : \nabla \otimes \nabla = \sum_{i,j=\{1,2,\ldots,d\}} v_i v_j \frac{\partial}{\partial x_i} \frac{\partial}{\partial x_j},$$

and $\mathbf{b}(\mathbf{x})$ is a drift term given by

$$\mathbf{b}(\mathbf{x}) = \int \mathbf{v}\, q(\mathbf{x}, \mathbf{v}) d\mathbf{v}. \quad (6)$$

If $q(\mathbf{x}, \mathbf{v}) = q(\mathbf{x}, -\mathbf{v})$ reorientation is symmetric in $\mathbf{v}$ and $\mathbf{b}(\mathbf{x}) = 0$ [38]. We now fix the speed $v = \sigma$. For $d = 1$ Eqs. 1 and 2 yield the telegrapher's equations with $q(x, \sigma) = q(x, -\sigma) = 1/2$ [39–43]. For $d > 1$, we set $\mathbf{v} = \sigma\, \hat{\theta}$, where $\hat{\theta}$ is the unit vector along the direction of motion. We write $q(\mathbf{x}, \mathbf{v}) = q(\mathbf{x}, \hat{\theta})\, \delta(v - \sigma)/\sigma^{d-1}$ where $q(\mathbf{x}, \hat{\theta})$ is the reorientation distribution and denote the angular volume element $d\hat{\theta}_{d-1}$ so that $\int q(\mathbf{x}, \hat{\theta}) d\hat{\theta}_{d-1} = \int q(\mathbf{x}, \mathbf{v}) d\mathbf{v} = 1$ and $\mathbf{b}(\mathbf{x}) = \sigma \int \hat{\theta} q(\mathbf{x}, \hat{\theta}) d\hat{\theta}_{d-1}$. Using the non-dimensional variables $\boldsymbol{\xi} = \mathbf{x}/L$, $\tau = \sigma^2 t/(\mu L^2)$, with L a typical length scale, we rewrite Eq. 2 as

$$\varepsilon^2 \frac{\partial S}{\partial \tau} - \varepsilon\, \hat{\theta} \cdot \nabla_{\boldsymbol{\xi}} S = -S + \int q(\boldsymbol{\xi}, \hat{\theta}) S(\boldsymbol{\xi}, \hat{\theta}, \tau) d\hat{\theta}_{d-1}. \quad (7)$$

Here, $\varepsilon = \ell/L$ is the Knudsen number and $\ell = \sigma/\mu$ the mean free path. We now assume $\varepsilon \ll 1$. Due to the drift term, a standard asymptotic expansion is insufficient, so we separate fast and slow time scales by introducing $z = \tau/\varepsilon$ and pose $S(\boldsymbol{\xi}, \hat{\theta}, \tau) = S_0(\boldsymbol{\xi}, \hat{\theta}, \tau) + \varepsilon S_1(\boldsymbol{\xi}, \hat{\theta}, \tau) + \ldots$ where $S_i(\boldsymbol{\xi}, \hat{\theta}, \tau) = s_i(\boldsymbol{\xi}, \hat{\theta}, \tau, z)$ [44]. The initial condition $S(\mathbf{x}, \mathbf{v}, 0) = 1$ for all $\mathbf{x}$ in $\mathcal{D}$ for any $\mathbf{v}$ maps to $s_i(\boldsymbol{\xi}, \hat{\theta}, 0, 0) = 0$ for $i \neq 0$ and $s_0(\boldsymbol{\xi}, \hat{\theta}, 0, 0) = 1$. Thus,

$$\frac{\partial S}{\partial \tau} = \frac{1}{\varepsilon} \frac{\partial s_0}{\partial z} + \left(\frac{\partial s_0}{\partial \tau} + \frac{\partial s_1}{\partial z} \right) + \ldots \quad (8)$$

By inserting Eq. 8 into Eq. 7, matching orders in ε and returning to τ, we find that $S_0(\boldsymbol{\xi}, \tau)$ is independent of $\hat{\theta}$ and that the integral $\int_0^\infty S_0(\boldsymbol{\xi}, \tau) d\tau$ satisfies a self-consistent differential equation. This integral is the rescaled MFPT to leading order. Rewriting it in dimensional units, $T(\mathbf{x}) = (\mu L^2/\sigma^2) \int_0^\infty S_0(\mathbf{x}, \tau) d\tau$, yields a self-consistent differential equation for $T(\mathbf{x})$, valid for $\varepsilon \ll 1$, given by

$$\mathbb{D}(\mathbf{x}) : \nabla \otimes \nabla\, T(\mathbf{x}) + \mathbf{b}(\mathbf{x}) \cdot \nabla\, T(\mathbf{x}) = -1, \quad (9)$$

where the diffusion tensor $\mathbb{D}(\mathbf{x})$ is defined as

$$\mathbb{D}(\mathbf{x}) = \frac{\sigma^2}{\mu} \int q(\mathbf{x}, \hat{\theta}) \hat{\theta} \otimes \hat{\theta}\, d\hat{\theta}_{d-1}, \quad (10)$$

and $T(\mathbf{x}) = 0$ at the target. Eq. 9 is one of our main findings and coincides with Eq. 5 for $v = \sigma$ and $\Theta(\mathbf{x}, \mathbf{v}) = T(\mathbf{x})$. It is more general than previous results as it allows directional asymmetries and a non-zero drift. More details are in the SM. Locally, interpreting L as the distance between the starting point and the target, Eq. 9 implies that the MFPT is independent of the initial orientation if the distance to the target is much larger than the mean free path. In this case, the many particle reorientations erase memory of the initial heading. The full kinetic description in Eq. 5 must be retained if instead the initial

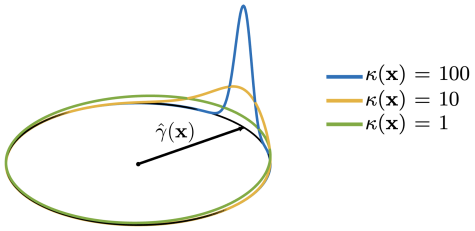

FIG. 1. The von Mises angular distribution in Eq. 11 for $d = 2$ and three values of the concentration $\kappa(\mathbf{x})$ that quantifies the bias towards $\hat{\gamma}(\mathbf{x})$. Larger $\kappa(\mathbf{x})$ yields sharper alignment.

TABLE I. Bias terms $\alpha(\mathbf{x}), \beta(\mathbf{x})$ for representative reorientation distributions $q(\mathbf{x},\cdot)$ that direct motion towards $\hat{\gamma}(\mathbf{x})$ through the concentration $\kappa(\mathbf{x})$ [45]. For $d=2$, $q(\mathbf{x},\cdot)=q(\mathbf{x},\hat{\theta})=q(\mathbf{x},\theta)$; for $d=3$, $q(\mathbf{x},\cdot)=q(\mathbf{x},\hat{n})$, where, respectively, $\hat{\theta}=(\cos\theta,\sin\theta)$ and $\hat{n}=(\sin\theta\cos\phi,\sin\theta\sin\phi,\cos\theta)$. For set boundary conditions, the MFPT is approximated by Eqs. 9, 12a, 12b, $D=\sigma^2/(d\mu)$.

distribution	$q(\mathbf{x},\cdot)$	$\alpha(\mathbf{x})$	$\beta(\mathbf{x})$
von Mises (2D)	$q_{\rm M}(\mathbf{x},\theta)=\dfrac{e^{\kappa(\mathbf{x})\cos(\theta-\gamma(\mathbf{x}))}}{2\pi I_0(\kappa(\mathbf{x}))}$	$\dfrac{I_2(\kappa(\mathbf{x}))}{I_0(\kappa(\mathbf{x}))}$	$\dfrac{I_1(\kappa(\mathbf{x}))}{I_0(\kappa(\mathbf{x}))}$
Fisher (3D)	$q_{\rm F}(\mathbf{x},\hat{n})=\kappa(\mathbf{x})\dfrac{e^{\kappa(\mathbf{x})\hat{\gamma}(\mathbf{x})\cdot\hat{n}}}{4\pi\sinh(\kappa(\mathbf{x}))}$	$1-\dfrac{3}{\kappa(\mathbf{x})}\coth(\kappa(\mathbf{x}))+\dfrac{3}{\kappa^2(\mathbf{x})}$	$\coth(\kappa(\mathbf{x}))-\dfrac{1}{\kappa(\mathbf{x})}$
wrapped Cauchy (2D)	$q_{\rm C}(\mathbf{x},\theta)=\dfrac{\operatorname{sech}(2\kappa(\mathbf{x}))}{2\pi(1-\tanh(2\kappa(\mathbf{x}))\cos(\theta-\gamma(\mathbf{x})))}$	$\tanh^2(\kappa(\mathbf{x}))$	$\tanh(\kappa(\mathbf{x}))$
Elliptical (2D)	$q_{\rm E}(\mathbf{x},\theta)=\dfrac{\operatorname{sech}^3(\kappa(\mathbf{x}))}{2\pi(1-\tanh(\kappa(\mathbf{x}))\cos(\theta-\gamma(\mathbf{x})))^2}$	$1-2\,\mathrm{cosech}^2(\kappa(\mathbf{x}))(1-\operatorname{sech}(\kappa(\mathbf{x})))$	$\tanh(\kappa(\mathbf{x}))$

position is at $\mathcal{O}(\ell)$ from the target. For isotropic reorientations, $q(\mathbf{x},\hat{\theta})=1/S_{\rm d}$, where $S_{\rm d}=2\pi^{d/2}/\Gamma(d/2)$ is the surface area of the unit $d-1$ sphere. A direct calculation yields $\mathbf{b}(\mathbf{x})=0$ and $\mathbb{D}(\mathbf{x})=D\,\mathbb{I}$, where $D=\sigma^2/(d\mu)$ and $\mathbb{I}$ are, respectively, the diffusion constant and identity matrix. Thus, Eq. 9 reduces to the standard diffusive MFPT equation $D\,\nabla^2 T(\mathbf{x})=-1$. We now evaluate $T(\mathbf{x})$ in $d=2$ for the von Mises distribution, the circular analog of a Gaussian, that biases reorientations towards a preferred direction [46–48]

$$q_{\rm M}(\mathbf{x},\hat{\theta})=q_{\rm M}(\mathbf{x},\theta)=\frac{e^{\kappa(\mathbf{x})\cos(\theta-\gamma(\mathbf{x}))}}{2\pi I_0(\kappa(\mathbf{x}))}. \tag{11}$$

Here, $\hat{\theta}=(\cos\theta,\sin\theta)$, $I_i(\cdot)$ is the modified Bessel function of the first kind of order i, $\hat{\gamma}(\mathbf{x})=(\cos\gamma(\mathbf{x}),\sin\gamma(\mathbf{x}))$ is the preferred direction at $\mathbf{x}$, and $\kappa(\mathbf{x})\geq 0$ is a unitless concentration parameter, which quantifies the degree of bias towards $\hat{\gamma}(\mathbf{x})$. The diffusion tensor and drift are

$$\mathbb{D}(\mathbf{x}) \;=\; D\,(1-\alpha(\mathbf{x}))\,\mathbb{I}+2D\alpha(\mathbf{x})\hat{\gamma}(\mathbf{x})\otimes\hat{\gamma}(\mathbf{x}) \tag{12a}$$

$$\mathbf{b}(\mathbf{x}) \;=\; \sigma\beta(\mathbf{x})\hat{\gamma}(\mathbf{x}) \tag{12b}$$

where the spatial dependence of $\alpha(\mathbf{x})$ and $\beta(\mathbf{x})$ is through $\kappa(\mathbf{x})$ as shown in Table I. In the weak-bias limit $\kappa\to 0$, $q_{\rm M}(\mathbf{x},\theta)$ becomes uniform; in the strong-bias limit $\kappa\to\infty$, $q_{\rm M}(\mathbf{x},\theta)$ approaches a Dirac-delta along $\hat{\gamma}(\mathbf{x})$. Further discussions of Eq. 11 and its limits are in the SM. Since $0\leq\alpha(\kappa),\beta(\kappa)<1$ are monotonically increasing in κ, they can be used as indicators of the strength of the bias along $\hat{\gamma}(\mathbf{x})$; when both approach zero, the diffusive MFPT equation is recovered; when both approach unity, motion is perfectly ballistic along $\hat{\gamma}(\mathbf{x})$. Remarkably, the same structure shown in Eqs. 12a and 12b emerges for other directed distributions in $d=2$ and for the Fisher distribution, the analogue of the von Mises distribution in $d=3$, provided all corresponding quantities are interpreted accordingly. We list these distributions in Table I with the corresponding bias terms $\alpha(\mathbf{x}),\beta(\mathbf{x})$. For all of them, $\kappa(\mathbf{x})$ interpolates between the uniform ($\kappa(\mathbf{x})\to 0$) and Dirac-delta ($\kappa(\mathbf{x})\to\infty$) distributions. While Eqs. 9, 12a, 12b are valid for any preferred direction, simple geometries and specific choices for $\hat{\gamma}(\mathbf{x})$ allow for simplifications. Typical ecological or biological scenarios involve finding the MFPT $T(\mathbf{x})$ to the boundary of a circular ($d=2$) or spherical ($d=3$) domain of radius R_0 for preferentially radial motion so that $\hat{\gamma}(\mathbf{x})=\pm\hat{r}$. If $\kappa(\mathbf{x})=\kappa(r)$ is radially symmetric, then so is $T(\mathbf{x})=T(r)$. Eq. 9 becomes

$$\frac{[1+\alpha(r)]}{2r^{d-1}}[r^{d-1}T'(r)]' - \frac{(d-1)\alpha(r)}{r}T'(r)\pm\frac{d\mu}{2\sigma}\beta(r)T'(r) \;=\; -\frac{1}{2D} \tag{13}$$

with $T(R_0)=0$. Here the plus (minus) sign indicates motion biased towards the positive (negative) radial direction $\hat{\gamma}(\mathbf{x})=\hat{r}$ ($\hat{\gamma}(\mathbf{x})=-\hat{r}$) and $\alpha(r),\beta(r)$ dictate the bias level. For all distributions listed in Table I, the limit $\kappa(r)\to 0$ leads to uniformly distributed reorientation angles, $\alpha(r),\beta(r)\to 0$ and Eq. 13 is solved by the purely diffusive form $T(r)=(R_0^2-r^2)/(2dD)$. The limit $\kappa(r)\to\infty$ instead leads to sharply peaked reorientation distributions, $\alpha(r),\beta(r)\to 1$ and Eq. 13 is solved by the purely ballistic form $T(r\neq R_0)=(R_0\mp r)/\sigma$. For $d=2$, the MFPT under tangential bias, $\hat{\gamma}(\mathbf{x})=\hat{r}^{\perp}$, satisfies

$$\frac{[1-\alpha(r)]}{2r}[rT'(r)]'+\frac{\alpha(r)}{r}T'(r)=-\frac{1}{2D}, \tag{14}$$

independently of the sign of the bias. Eqs. 13 and 14 can be solved exactly for any radially symmetric boundary conditions. The MFPT to exit an annulus ($d=2$) or a spherical shell ($d=3$) defined by $\rho\leq r\leq R_0$ from either or both inner and outer boundaries is given by

$$T(r) \;=\; H_1+\int^r e^{-\mathcal{F}(\eta)}d\eta\left[H_2-\frac{1}{D}\int^{\eta}\frac{e^{\mathcal{F}(s)}}{1+z\alpha(s)}ds\right] \tag{15}$$

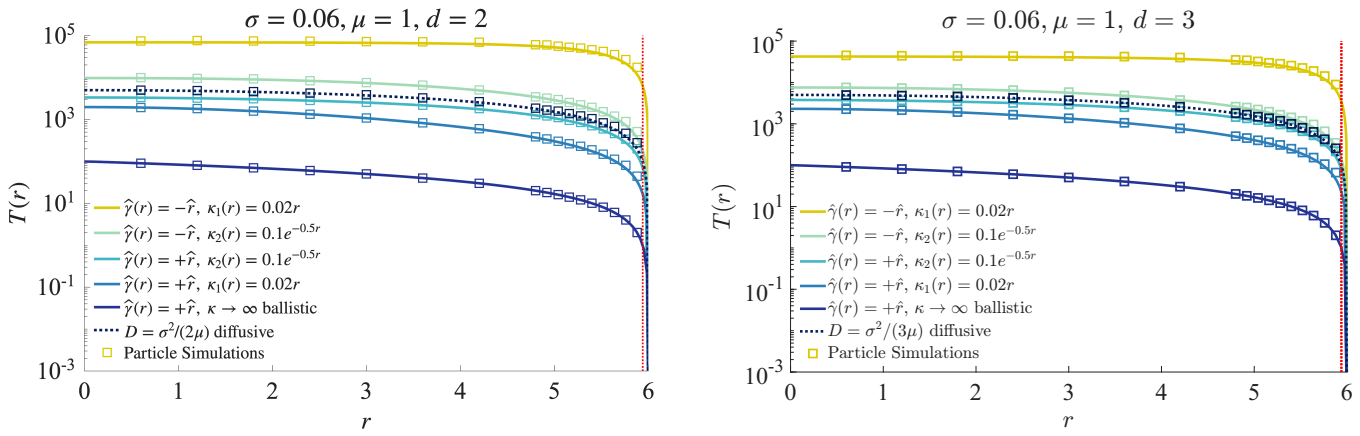

FIG. 2. Analytical estimates from Eq. 15 (curves) and particle simulations (squares) of the MFPT to the boundary of a ball of radius $R_0 = 6$ in $d = 2$ (left) and $d = 3$ (right). Reorientations follow the von Mises ($d = 2$) or Fisher ($d = 3$) distributions given in Table I. The speed $\sigma = 0.06$ and turning rate $\mu = 1$ yield the diffusion constant $D = \sigma^2/(d\mu)$, mean free path $\ell = \sigma/\mu = 0.06$, and Knudsen number $\varepsilon = \ell/R_0 = 0.01$. Deviations may arise when the initial distance to the exit boundary is comparable to ℓ, i.e. for $r \gtrsim R_0 - \ell = 5.94$, denoted by the red vertical line. For unbiased motion (black dotted curves), when $\kappa(r) = \alpha(r) = \beta(r) = 0$, the diffusive form $T(r) = (R_0^2 - r^2)/(2dD)$ is recovered from Eq. 15. In all other curves motion is biased along the positive or negative radial direction $\hat{\gamma}(r) = \pm\hat{r}$ via $\kappa_1(r) = r/\lambda_1$ (increasing as the boundary is approached) or $\kappa_2(r) = Ae^{-r/\lambda_2}$ (decreasing as the boundary is approached). The limit $\kappa(r) \to \infty$, $\gamma(r) = \hat{r}$, $\alpha(r), \beta(r) \to 1$ yields the ballistic form $T(r) = (R_0 - r)/\sigma$. Compared to purely diffusive trajectories, positive biases reduce the MFPT, negative biases induce detours that delay exit. Even relatively modest biases can alter the MFPT by several orders of magnitude. We set $A = 0.1, \lambda_1 = 50, \lambda_2 = 2$. Simulations are averaged over 10^4 runs. Units are arbitrary. Other parameter choices are in the SM.

where $z = 1$ for radial bias ($d = 2, 3$), $z = -1$ for tangential bias ($d = 2$), the integration constants H_1, H_2 depend on the chosen exit conditions, and

$$\mathcal{F}(r) = \int^r \frac{(d-1)}{s}\frac{1 - z\alpha(s)}{1 + z\alpha(s)} \pm \frac{z+1}{2\sigma}\frac{d\mu\beta(s)}{1+\alpha(s)}\, ds. \quad (16)$$

In Fig. 2 we compare analytical estimates to numerical simulations of the MFPT for particles following the von Mises ($d = 2$) or Fisher ($d = 3$) distributions with preferred orientation $\hat{\gamma} = \pm\hat{r}$ and exiting a disk ($d = 2$) or sphere ($d = 3$) at $r = R_0$. This corresponds to $z = 1$, $\rho = 0$ in Eq. 15 where H_1, H_2 are determined from $T'(0) = T(R_0) = 0$. We choose $\kappa(r) \to 0$ (standard diffusion), $\kappa(r) \to \infty$ (ballistic motion) and two non-uniform concentrations $\kappa_1(r) = r/\lambda_1$, where the bias increases as the boundary is approached, and $\kappa_2(r) = A\, e^{-r/\lambda_2}$, where the opposite is true. If we identify L with R_0, the parameters used in Fig. 2 yield $\varepsilon = \ell/R_0 = 0.01$. As shown, simulations and estimates from Eq. 15 are in excellent agreement. Locally, we expect deviations only in the thin layer $R_0 - r \lesssim \ell$ when the distance to the boundary is $\mathcal{O}(\ell)$. Fig. 2 also shows that $T(r)$ is highly sensitive to bias, as even slight directional preferences can lead to dramatic departures from the standard diffusive MFPT. Relative to isotropic diffusion, biases in the positive radial direction shorten the MFPT, biases in the opposite direction delay it.

Of particular interest is the narrow capture problem, where a particle seeks a small target in a larger domain [12, 49]. We assume that the particle is initiated at $\rho < r < R_0$ and follows the von Mises ($d = 2$) or Fisher ($d = 3$) distributions with uniform κ (and uniform α, β as per Table I) under radial bias. We first take the bulk limit $\ell/\rho \to 0^+$, so that for $r \gtrsim \rho + \ell$, $T(r)$ is found by solving Eq. 15 with $z = 1$ and $T(\rho) = T'(R_0) = 0$. We then take the narrow-capture limit $\rho/R_0 = \zeta \to 0^+$, effectively enlarging the bulk and further suppressing boundary effects. The derived $T(r)$ is used to approximate the global MFPT $\tau_{\rm g}$, defined as spatial average of the MFPT, $\tau_{\rm g} \sim |\mathcal{D}|^{-1}\int_{\mathcal{D}} T(r) r^{d-1} dr$, leading to the scaling form

$$\tau_{\rm g} \sim C_{\rm r}\, \zeta^{\frac{d(\alpha-1)+2}{\alpha+1}}(1 + \mathcal{O}(\zeta)), \qquad \zeta \to 0^+. \quad (17)$$

This anomalous scaling differs markedly from the standard diffusive forms $\tau_{\rm g} \sim \log\zeta$ ($d = 2$) and $\tau_{\rm g} \sim \zeta^{-1}$ ($d = 3$); in particular, $\tau_{\rm g}$ remains finite as $\zeta \to 0^+$ for all $\alpha > 0$ in $d = 2$ and for $\alpha > 1/3$ in $d = 3$. The corresponding κ can be found via Table I. For tangential bias in $d = 2$, a similar approach with $z = -1$ in Eq. 15 yields

$$\tau_{\rm g} \sim C_{\rm t}\, \zeta^{-\frac{2\alpha}{1-\alpha}}(1 + \mathcal{O}(\zeta)), \qquad \zeta \to 0^+, \quad (18)$$

so that $\tau_{\rm g}$ diverges for all $0 < \alpha < 1$, another striking departure from standard diffusion. For $\zeta \to 0$, bulk transport dominates and boundary layer effects will modify only prefactors, not scaling exponents. Higher moments $T_n(\mathbf{x}) = n(\mu R_0^2/\sigma^2)^n \int_0^\infty t^{n-1} S_0(\mathbf{x}, \tau) d\tau$ can also be derived from Eq. 7 to leading order in ε via the hierarchy

$$\mathbb{D}(\mathbf{x}) : \nabla \otimes \nabla\, T_n + \mathbf{b}(\mathbf{x}) \cdot \nabla\, T_n = -nT_{n-1} \quad (19)$$

where $n > 1$ and $T_1(\mathbf{x}) \equiv T(\mathbf{x})$ is the MFPT. Eq. 19 is valid for all $d = 2, 3$ distributions in Table I.

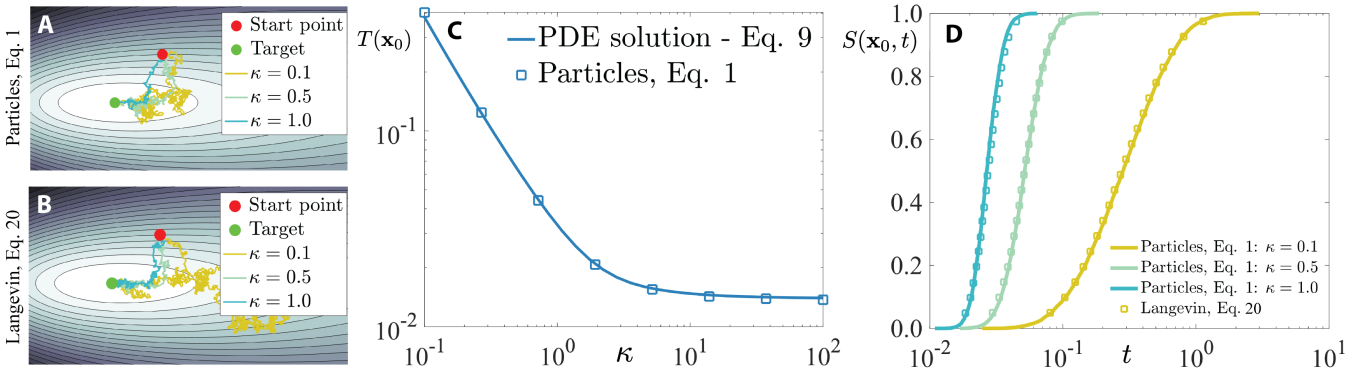

FIG. 3. Two-dimensional particles searching for the locus $\mathbf{x}_T$ of maximal concentration of the Gaussian plume $\phi(\mathbf{x}) = Q/(2\pi Kx)e^{-u(y^2+H^2)/(4Kx)}$ with $Q = 2$, $K = 0.5$, $u = 5$, $H = 1$ and $\mathbf{x}_T = (uH^2/4K, 0) = (2.5, 0)$. Particles start at $\mathbf{x}_0 = (3, 0.5)$ and follow the von Mises distribution in Eq. 11 with $\hat{\gamma}(\mathbf{x}) = \nabla\phi(\mathbf{x})/|\nabla\phi(\mathbf{x})|$ and uniform κ. Speed and turning rate are $\sigma = \sqrt{\mu} = 10^2$. The trajectories in panels A,B, derived from Eq. 1 and the Langevin process in Eq. 20 respectively, are qualitatively similar. Panel C shows strong agreement between the MFPT $T(\mathbf{x}_0)$ from Eq. 9 and simulations of Eq. 1 averaged over 10^4 runs. Panel D shows that Eq. 20 accurately captures the survival probability $S(\mathbf{x}_0, t)$. Units are arbitrary.

Upon expressing Eq. 9 in operator form, $\mathcal{L}^* T(\mathbf{x}) = -1$, and using Itô's interpretation, we infer the following Langevin process

$$d\mathbf{x} = \mathbf{b}(\mathbf{x})dt + [2\mathbb{D}(\mathbf{x})]^{\frac{1}{2}} dW_t, \tag{20}$$

where $\mathbf{b}(\mathbf{x}), \mathbb{D}(\mathbf{x})$ are as in Eqs. 12a, 12b, the root is taken in the matrix sense, and W_t is a vector of Brownian motions. For $\varepsilon \ll 1$ and by construction, the velocity jump and Langevin processes display identical first-passage statistics; Eq. 20 allows for the exploration of additional dynamical properties. As an example, we consider a random walker seeking the locus $\mathbf{x}_\mathrm{T}$ of maximal concentration of a given plume $\phi(\mathbf{x})$ in $d = 2$. We let the walker follow the von Mises distribution in Eq. 11 with uniform κ and preferred direction given by the normalized gradient of $\phi(\mathbf{x})$, $\hat{\gamma}(\mathbf{x}) = \nabla\phi(\mathbf{x})/|\nabla\phi(\mathbf{x})|$. For concreteness, we choose $\phi(\mathbf{x})$ as the planar projection at steady state of a Gaussian plume generated at altitude H, at constant rate Q, advected at speed u along the x-direction, and dispersed with diffusion constant K, leading to $\phi(\mathbf{x}) = Q/(2\pi Kx)e^{-u(y^2+H^2)/(4Kx)}$ [50]; this plume is maximal at $\mathbf{x}_\mathrm{T} = (uH^2/4K, 0)$. Representative trajectories from simulations of particles starting at $\mathbf{x}_0$ following Eq. 1 or the Langevin dynamics in Eq. 20 are shown in Figs. 3A and 3B, respectively. The corresponding MFPTs to $\mathbf{x}_\mathrm{T}$, calculated from Eq. 1, are displayed in Fig. 3C as a function of κ and show excellent agreement with solutions to Eq. 9. As seen in Fig. 3D, the Langevin process in Eq. 20 yields the full survival probability $S(\mathbf{x}_0, t)$, and not just the MFPT $T(\mathbf{x}_0)$, with remarkable accuracy.

Our results have broad applications. As shown in the SM, the von Mises kernel in Eq. 11 is the steady-state distribution of an overdamped angular system driven by the potential $U(\theta, \mathbf{x}) = -\tau_\mathrm{M}(\mathbf{x})\cos(\theta - \gamma(\mathbf{x}))$, where the torque biases orientation along $\hat{\gamma}(\mathbf{x})$ in competition with rotational noise [51], leading to $\kappa(\mathbf{x}) \propto \tau_\mathrm{M}(\mathbf{x})$. Assuming an electric field of magnitude $E(\mathbf{x})$ directed along $\hat{\gamma}(\mathbf{x})$, we can model $\tau_\mathrm{M}(\mathbf{x}) \propto E(\mathbf{x})$, so that $\kappa(\mathbf{x}) \propto E(\mathbf{x})$. Thus, Eq. 11 arises as a natural way to describe field-driven motion. For $d = 2$, radial guidance and a uniform, weak E Eq. 17 yields $\tau_\mathrm{g} \sim \zeta^\nu$ with $\nu \propto E^2$, providing an avenue to test the predicted scaling. For behavioral systems, without physical torques, Eq. 11 can still be used to model transport biased by trails, social cues, or learning. From this perspective, as discussed in the SM, our work offers a unified framework in which to study the MFPT of field-driven colloidal matter, run-and-tumble bacteria under chemotaxis, active swimmers, and animal movement [52–66]. Finally, mapping the dynamics onto Eq. 20 allows to reconstruct the bias terms $\alpha(\mathbf{x})$ and $\beta(\mathbf{x})$ from experimentally observed trajectories.

In summary, we presented a novel theory for the MFPT of velocity jump processes in higher dimensions, whose general form is Eq. 5. For fixed speed and the angular distributions listed in Table I for $d = 2, 3$, we show that the capture statistics in the small Knudsen number limit are governed by the bias terms $\alpha(\mathbf{x})$ and $\beta(\mathbf{x})$ via Eq. 9, and can differ quite significantly from those observed under standard diffusion. Furthermore, the identification of a generator function for the underlying stochastic process leads to the Langevin approximation in Eq. 20 that efficiently describes the transport dynamics. We fixed particle speed and let directional persistence arise from the sharpness of the angular distribution. If particle speeds followed heavy-tailed distributions, as in Lévy processes, exceptionally large jumps could lead to rare boundary-reaching events. This scenario would require a different analysis than what presented here, invoking for example the "single big jump" principle [67]. Solving the full problem in Eq. 2 requires tracking both particle position and velocity. Appropriate boundary conditions must be

specified for $S(\mathbf{x}, \mathbf{v}, t)$, carefully distinguishing between inward and outward directions on the boundary, as shown in the SM. A full treatment is left for future work.

We thank T. Chou and K. Painter for fruitful discussions. This work was supported by the ARO (grant W911NF-23-1-0129, MRD), the NSF (grants DMS-2052636, AEL and OAC-2320846, MRD) and the NSERC (Discovery grant RGPIN-2023-04269, TH). The data that support the findings of this article are openly available [68].

* dorsogna@csun.edu

[1] N. G. van Kampen, *Stochastic Processes in Physics and Chemistry* (North-Holland, Amsterdam, 1981).
[2] R. Klages, G. Radons, and I. M. Sokolov, *Anomalous Transport* (John Wiley & Sons, 2008).
[3] P. Hänggi, P. Talkner, and M. Borkovec, *Rev. Mod. Phys.* **62**, 251 (1990).
[4] S. A. Iyaniwura and Z. Peng, *New J. Phys.* **27**, 104401 (2025).
[5] P. C. Bressloff and J. M. Newby, *Phys. Rev. E* **83**, 061139 (2011).
[6] A. Scacchi and A. Sharma, *Mol. Phys.* **116**, 460–464 (2018).
[7] A. Dhar, A. Kundu, S. N. Majumdar, S. Sabhapandit, and G. Schehr, *Phys. Rev. E* **99**, 032132 (2019).
[8] L. Angelani, R. Di Lionardo, and M. Paoluzzi, *Eur. Phys. J. E* **37**, 59 (2014).
[9] J. Perelló, M. Gutiérrez-Roig, and J. Masoliver, *Phys. Rev. E* **84**, 066110 (2011).
[10] J. Masoliver and J. Perelló, *Phys. Rev. E* **78**, 056104 (2008).
[11] T. R. Bielecki and M. Rutkowski, in *Credit Risk: Modeling, Valuation and Hedging* (Springer Finance, Berlin, Heidelberg, 2004).
[12] V. Kurella, J. C. Tzou, D. Coombs, and M. Ward, *Bull. Math. Biol.* **77**, 83–125 (2015).
[13] A. C. Costa, G. Sridhar, C. Wyart, and M. Vergassola, *PRX Life* **2**, 023001 (2024).
[14] P. Fauchald and T. Torkild, *Ecol.* **84**, 282–288 (2003).
[15] O. Bénichou, C. Loverdo, M. Moreau, and R. Voituriez, *Rev. Mod. Phys.* **83**, 81 (2011).
[16] O. Heaviside, *Electrical papers of Oliver Heaviside, volume I* (Chelsea, New York, 1970).
[17] L. Angelani, *J. Phys. A: Math. Theor.* **48**, 495003 (2015).
[18] T. Hillen and K. J. Painter, in *Dispersal, individual movement and spatial ecology* (Springer, 2013), pp. 177–222.
[19] T. Hillen, *Math. Models Methods Appl. Sci.* **12**, 1007–1034 (2002).
[20] A. Datta, C. Beta, and R. Großmann, *Phys. Rev. Res.* **6**, 043281 (2024).
[21] S. Redner, *A Guide to First-Passage Processes* (Cambridge University Press, 2001).
[22] K. R. Ghusinga, J. J. Dennehy, and A. Singh, *Proc. Natl. Acad. Sci.* **114**, 693–698 (2017).
[23] M. R. D'Orsogna and T. Chou, *PLoS One* **4**, e8165 (2009).
[24] S. A. Nowak and T. Chou, *Biophys. J.* **96**, 2624–2636 (2009).
[25] P. C. Bressloff and J. M. Newby, *Rev. Mod. Phys.* **85**, 135 (2013).
[26] S. Condamin, V. Tejedor, R. Voituriez, O. Bénichou, and J. Klafter, *Proc. Natl. Acad. Sci. USA* **105**, 5675 (2008).
[27] C. W. Gardiner, *Handbook of Stochastic Methods: for Physics, Chemistry and the Natural Sciences* (Springer Berlin, 2004).
[28] B. M. S. Arani, S. R. Carpenter, L. Lahti, E. H. van Nes, and M. Scheffer, *Science* **372**, eaay4895 (2021).
[29] S. Mao, T. Chou, and M. R. D'Orsogna, *Math. Biosci.* **372**, 109184 (2024).
[30] J. Klinger, R. Voituriez, and O. Bénichou, *Phys. Rev. E* **107**, 054109 (2023).
[31] B. A. Camley and W. J. Rappel, *Phys. Rev. E* **89**, 062705 (2014).
[32] A. Vezzani and R. Burioni, *Phys. Rev. Lett.* **132**, 187101 (2024).
[33] R. Artuso, G. Cristadoro, M. Onofri, and M. Radice, *J. Stat. Mech.* 2018, 083209 (2018).
[34] F. J. Sevilla, A. V. Arzola, and E. P. Cital, *Phys. Rev. E* **99**, 012145 (2019).
[35] D. S. Grebenkov, *Phys. Rev. Lett.* **117**, 260201 (2016).
[36] F. Mori, P. Le Doussal, S. N. Majumdar, and G. Schehr, *Phys. Rev. Lett.* **124**, 090603 (2020).
[37] J. F. Rupprecht, O. Bénichou, and R. Voituriez, *Phys. Rev. E* **94**, 012117 (2016).
[38] T. Hillen, M. R. D'Orsogna, J. Mantooth, and A. E. Lindsay, *SIAM Appl. Math.* **28**, 78–108 (2025).
[39] P. C. Hemmer, *Physica A* **27**, 79–82 (1961).
[40] M. Kac, *Rocky Mountain J. Math.* **4**, 497–510 (1974).
[41] M. R. D'Orsogna, M. Suchard, and T. Chou, *Phys. Rev. E* **68**, 021925 (2003).
[42] G. H. Weiss, *Aspects and Applications of the Random Walk* (North-Holland, Amsterdam, 1994).
[43] G. H. Weiss, *Physica A* **311**, 381–410 (2002).
[44] C. M. Bender and S. A. Orszag, *Advanced Mathematical Methods for Scientists and Engineers: Asymptotic Methods and Perturbation Theory* (Springer, New York, 1999).
[45] H. Wu, B. L. Li, T. A. Springer, and W. H. Neill, *Ecol. Model.* **132**, 115–124 (2000).
[46] T. Hillen, K. J. Painter, A. C. Swan, and A. Murtha, *Math. Biosci. Eng.* **14**, 673–694 (2017).
[47] I. Bica, T. Hillen, and K. J. Painter, *J. Theor. Biol.* **427**, 77–89 (2017).
[48] A. C. Swan, T. Hillen, J. Bowman, and A. Murtha, *Bull. Math. Biol.* **80**, 1259–1291 (2017).
[49] S. Chakraborty, T. Kolokolnikov, and A. E. Lindsay, *Eur. J. Appl. Math.* (2025), 1–25.
[50] J. M. Stockie, *SIAM Review* **53**, 349–371 (2011).
[51] F. Höfling and A. V. Straube, *Phys. Rev. Res.* **7**, 043034 (2025).
[52] T. Narazaki *et al.*, *iScience* **24**, 102221 (2021).
[53] M. N. Popescu, W. E. Uspal, C. Bechinger, and P. Fischer, *Nano Lett.* **18**, 5345–5351 (2018).
[54] H. Karani, G. E. Pradillo, and P. M. Vlahovska, *Phys. Rev. Lett.* **123**, 208002 (2019).
[55] E. Lauga, W. R. Di Luzio, G. M. Whitesides, and H. A. Stone, *Biophys. J.* **90**, 400–412 (2006).
[56] F. Kümmel, B. ten Hagen, R. Wittkowski, I. Buttinoni, R. Eichhorn, G. Volpe, H. Löwen, and C. Bechinger, *Phys. Rev. Lett.* **110**, 198302 (2013).
[57] T. C. Schneirla, *Am. Mus. Novit.* **1253**, 1–26 (1944).
[58] C. M. Buness, A. Rana, C. C. Maass, and R. Dey, *Phys.*

Rev. Lett. **133**, 158301 (2024).
[59] P. J. Mlynarczyk and S. M. Abel, *Phys. Rev. E* **99**, 022406 (2019).
[60] H. W. McKenzie, M. A. Lewis, and E. H. Merrill, *Bull. Math. Biol.* **71**, 107–129 (2009).
[61] T. M. Nieuwenhuizen, S. Klumpp, and R. Lipowsky, *Phys. Rev. E* **6**, 061911 (2004).
[62] A. Codutti, K. Bente, D. Faivre, and S. Klumpp, *PLoS Comput. Biol.* **15**, e1007548 (2019).
[63] E. Boissard, P. Degond, and S. Motsch, *J. Math. Biol.* **66**, 1267–1301 (2013).
[64] V. Sourjik and N. S. Wingreen, *Curr. Opin. Cell Biol.* **24**, 262–268 (2012).
[65] K. Saito, R. Kawano, C. Sadamatsu, Y. Iwashita, and Y. Kimura, *Phys. Rev. E* **111**, 045409 (2025).
[66] W. Wang, W. Duan, S. Ahmed, T. E. Mallouk, and A. Sen, *Nano Today* **8**, 531–554 (2013).
[67] A. Vezzani, E. Barkai, and R. Burioni, **100**, 012108 (2019).
[68] M. R. D'Orsogna, A. E. Lindsay, and T. Hillen, "MFPT code repository," `https://github.com/dorsogna/MFPT`, accessed March 30, 2026.